CHEMISTRY OF MATERIALS

ARTICLE

pubs.acs.org/cm

Facile Synthesis of Ordered Mesoporous Alumina and Alumina-Supported Metal Oxides with Tailored Adsorption and Framework Properties

Weiquan Cai,[†,‡] Jiaguo Yu,[‡,*] Chokkalingam Anand,[§] Ajayan Vinu,[§] and Mietek Jaroniec[*,†]

[†]Department of Chemistry, Kent State University, Kent, Ohio, 44242, United States

[‡]School of Chemical Engineering and State Key Laboratory of Advanced Technology for Material Synthesis and Processing, Wuhan University of Technology, Luoshi Road 122#, Wuhan 430070, People's Republic of China

[§]International Center for Materials Nanoarchitectonics, WPI Research Center, National Institute for Materials Science, 1-1 Namiki, Tsukuba 305-0044, Japan

Supporting Information

ABSTRACT: The evaporation-induced self-assembly (EISA) in ethanolic solution of a triblock copolymer (Pluronic P123) is explored for the synthesis of ordered mesoporous alumina (MA) and MA-supported metal oxides, using aluminum isopropoxide, aluminum chloride, and aluminum nitrate nonahydrate as aluminum precursors, and nickel, magnesium, iron, chromium, copper, cerium, lanthanum, yttrium, calcium, tin chlorides, or nitrates as metal precursors. The as-synthesized mesoporous oxides were characterized by a variety of techniques, such as thermogravimetry, Fourier transform infrared spectroscopy, nitrogen adsorption, small- and wide-angle X-ray diffraction, high-resolution transmission electron microscopy, energy-dispersive X-ray spectrometry, elemental mapping, and CO_2 and NH_3 temperature-programmed desorption. It is shown that the EISA strategy in the presence of polymeric template not only is well-suited for the synthesis of ordered MAs and MA-supported metal oxides with tailored adsorption and framework properties, but also ensures a homogeneous distribution of metal species within inorganic framework with the aluminum/metal atomic ratio close to this used in the synthesis mixture. The aluminum and other metal precursors used in EISA have a significant impact on the pore structure, surface area, and basic and acidic properties of the resulting mixed oxides. For instance, the use of inexpensive aluminum nitrate nonahydrate in the synthesis leads to the significantly enlarged mesopores (ranging from ~7 nm to 16 nm), improved ordering of the oxides, and enhanced adsorption affinity toward CO_2, while the aluminum chloride precursor affords MA-supported metal oxides with a bimodal pore size distribution, with peaks located in the ranges of 2−4 nm and 5−9 nm, respectively. It is also shown that the use of inexpensive aluminum and metal salts as precursors instead of aluminum alkoxides affords MA-supported metal oxides with tailorable properties, in terms of the surface area, porosity, and surface basicity and acidity, which determine the performance of these materials in various applications, including adsorption and catalysis.

KEYWORDS: porous materials, self-assembled materials, mesoporous alumina, mixed metal oxides

1. INTRODUCTION

Alumina is of great interest for a variety of applications, because of its unique catalytic, adsorption, optical, and electronic properties; thus, the control of physicochemical properties of this material is the key topic of ongoing research.[1−5] In particular, mesoporous aluminas (MAs) with uniform pores, high surface area, and narrow pore-size distribution are highly desirable for many of the aforementioned applications.[6,7] In comparison to the remarkable advancements in the area of mesostructured silicas, a limited progress has been made in the synthesis of MAs.[8,9] The recipes, normally used for the synthesis of mesoporous silica, do not work well for alumina, because of the fast hydrolysis and condensation rates of aluminum alkoxides.[10] The first successful synthesis of ordered MA from aluminum *sec*-butoxide was achieved by Vaudry et al.,[11] using long-chain carboxylic acids as the structure directing agents in low-molecular-weight alcoholic solvents. So far, the existing recipes for the synthesis of ordered MAs are based mainly on the sol−gel self-assembly processes in the presence of both soft (cationic, anionic, and nonionic surfactants) and hard (polymers and carbon molds) templates.[7] A remarkable way of achieving the growth of ordered MA structures is the solvent evaporation-induced self-assembly (EISA) allowing fine-tuning of structural properties of these materials.[12−16] The EISA strategy can competently replace the process of cooperative assembly of precursors and surfactant templates, which is normally used for the preparation of mesoporous materials, especially in the case of nonsiliceous mesoporous materials.[17]

There is an ongoing dispute on the importance of ordered versus disordered mesostructures for various applications.

Received: September 1, 2010
Revised: December 11, 2010
Published: January 20, 2011

dx.doi.org/10.1021/cm102512v | *Chem. Mater.* 2011, 23, 1147–1157

The superiority of three-dimensional (3D) wormhole-like (disordered) mesostructures over hexagonally ordered ones has been observed by some researchers, with regard to the enhanced accessibility of the active sites by reactant molecules, which is essential for catalytic performance.[18] Some exemplary applications of disordered MA-based catalysts show their higher activity in hydrodesulfurization, hydrodechlorination, metathesis, and some oxidation reactions, in comparison to those based on conventional aluminas.[6,7] On the other side, highly ordered MAs with large surface areas (ca. 400 m^2/g), high pore volumes (ca. 0.70 cm^3/g), and tunable pore sizes have been shown to exhibit the desired reactant size selectivity in the hydrogenation of acetone, D-glucose, and D-(+)-cellobiose, indicating its potential applications in shape-selective catalysis.[15] Therefore, judging which of the two aforementioned MA structures is superior remains difficult. Most likely, the development of both types of MA—ordered and disordered mesostructures—is desired to satisfy the diverse requirements of a wide variety of applications.[17]

Recently, ordered MA-supported metal oxides have emerged as a new group of functional materials with enhanced catalytic activity and selectivity.[19] In comparison to the wet impregnation of MA with metal oxide precursors, which often leads to structure blockage and/or damage, the one-pot synthesis of MA-supported metal oxides is suitable to achieve high-quality mesostructures that exhibit strong metal−support interactions and retain homogeneous distribution of active sites.[20] For example, the nickel-containing MA catalyst prepared by a post-hydrolysis method exhibited smaller nickel particles and was less susceptible to carbon deposition, which resulted in better catalytic activity than that of the nickel catalyst impregnated directly on a MA.[21] Furthermore, in comparison to pure ordered MAs, the incorporation of metal species into the MA structure during one-pot synthesis may result in larger and accessible mesopores, improved thermal stability, and higher loading of catalytically active metal oxides, which are essential features for many applications.[22] However, the recently proposed combination of the sol−gel process with EISA in the presence of the Pluronic P123 polymeric template to synthesize MA-supported metal oxides in ethanol is highly dependent on the aluminum alkoxide and the added nitric acid as a coordination agent and pH adjuster. Especially, from the environmental and economical viewpoints, inorganic aluminum salts are inexpensive and easily available; thus, they are more-attractive precursors than expensive and toxic aluminum alkoxides. Therefore, there is still a great interest in preparing ordered MA and MA-supported metal oxides with uniform pores, narrow pore size distributions, high surface areas, and large pore volumes, using various aluminum salts.

Based on the EISA and soft-templating strategies we propose a feasible approach to the synthesis of MA with ordered and disordered mesostructures by changing aluminum precursors and using Pluronic P123 block copolymer as a soft template without adding any acid. The successful synthesis of ordered MA-supported metal oxides with Ni, Mg, Fe, Cr, Cu, Ce, La, Y, Ca, and Sn demonstrates the generality of this approach. Importantly, the partially ordered MAs and MA-supported metal oxides, which exhibit large mesopores and excellent CO_2 adsorption performance, can be prepared using hydrated aluminum nitrate as a precursor.

2. EXPERIMENTAL SECTION

2.1. Synthesis of Ordered MAs and MA-Supported Metal Oxides. Ordered MA and MA- supported metal oxides were synthesized using an extensively modified recipe based on those reported by Zhao, Jaroniec, and their co-workers.[13,22] All reagents were analytical-grade, supplied by Acros Organics, and used as received without further purification, except for $(EO)_{20}(PO)_{70}(EO)_{20}$ triblock copolymer (Pluronic P123) (from BASF, Co.), $CrCl_3$ (from Matherson Coleman and Bell), and commercial boehmite powder (Catapal A, from Sasol). In a typical synthesis, 1.0 g of Pluronic P123 and 0.3789 g of $Al(NO_3)_3\cdot 9H_2O$ were successively added to 20 mL of anhydrous ethanol in a 250-mL polypropylene wide-mouth bottle, and the resultant mixture was vigorously stirred at 40 °C for 70 min. Then, 2.0842 g of aluminum isopropoxide ($Al(OC_3H_7)_3$) was slowly added to the above solution and the mixture was sealed again and further stirred at 40 °C for 6 h. The final solution was transferred to an oven and underwent solvent evaporation at 60 °C for 48 h in static air. Under these conditions, ethanol was gradually evaporated, and the wet gel was finally converted to xerogel. The resulting xerogel was calcined at 400 °C for 4 h in flowing air to remove the template. Calcination was performed in a horizontal quartz tube furnace with a heating rate of 1 °C/min. The other syntheses of MAs were performed analogously, using different mixed and single precursors: $Al(OC_3H_7)_3-AlCl_3$, $Al(NO_3)_3\cdot 9H_2O-AlCl_3$, $AlCl_3-Al(NO_3)_3\cdot 9H_2O$, $Al(NO_3)_3\cdot 9H_2O$, and $AlCl_3$. The quantities of the former and latter components in the pair of precursors were 0.01 and 0.001 mol, respectively.

To illustrate the generality of this approach, a series of alumina-supported metal oxides was synthesized, in which a 10% molar ratio of metal species to aluminum (0.01 mol) was added. Precursors for Ni-, Mg-, Fe-, Cr-, Cu-, Ce-, La-, Y-, Ca-, and Sn-containing species were $Ni(NO_3)_2\cdot 6H_2O$ and $NiCl_2\cdot 6H_2O$, $Mg(NO_3)_2\cdot 6H_2O$, $Fe(NO_3)_3\cdot 9H_2O$ and $FeCl_3$, $CrCl_3$, $Cu(NO_3)_2\cdot 3H_2O$ and $CuCl_2\cdot 2H_2O$, $CeCl_3\cdot 7H_2O$, $LaCl_3\cdot 6H_2O$, $YCl_3\cdot 6H_2O$, $Ca(NO_3)_2\cdot 4H_2O$, and $SnCl_4\cdot 3H_2O$, respectively. The metal precursor was added to the Pluronic P123 solution of ethanol before addition of the key aluminum precursor. The other steps of the synthesis were the same as those given in the above-described recipe for the preparation of MA.

The final samples were labeled, starting with a prefix of MA followed by the type of aluminum precursors (i, n, and c, which refer to aluminum isopropoxide, aluminum nitrate nonahydrate, and aluminum chloride, respectively), then by metal (Me), and finally its precursors (if two salts were used as precursors for the same metal, Me and Me* refer to nitrate and chloride, respectively). For example, MA-i-Ni refers to a Ni-Al oxide prepared from $Al(OC_3H_7)_3$ and $Ni(NO_3)_2\cdot 6H_2O$ with a 10% molar ratio of Ni/Al calcined at 400 °C for 4 h in flowing air.

2.2. Characterization. Thermogravimetry/differential thermogravimetry (TG/DTG) analysis was performed on a TA Instruments Hi-Res TGA 2950 thermogravimetric analyzer, using a high-resolution mode. The curves were recorded in flowing air with a heating rate of 5 °C/min up to 840 °C. Powder X-ray diffraction (XRD) measurements were performed using an X'Pert Pro MPD multipurpose diffractometer (PANalytical, Inc.) with Cu Kα radiation (0.15406 nm) at room temperature from 0.4° to 5.0° (small angle) and from 10.0° to 80.0° (wide angle). Measurements were conducted using a voltage of 40 kV, a current setting of 40 mA, a step size of 0.02°, and count times of 4 s (wide angle) and 20 s (small angle). Microscope glass slides were used as sample supports for all samples. Fourier-transform infrared (FT-IR) spectra were collected using a Bruker Model Vector 22 FT-IR spectrometer in the frequency range of 4000−500 cm^{-1}. Nitrogen adsorption isotherms were measured at −196 °C on ASAP 2010 and 2020 volumetric analyzers (Micromeritics, Inc., Norcross, GA). Prior adsorption measurements all samples were outgassed under vacuum at 120 °C for 2 h. HRTEM images were obtained with JEOL Model JEM-2100F. The accelerating voltage of the electron beam was 200 kV. The preparation of samples for HRTEM analysis involved sonication in ethanol for 2−5 min and deposition on a copper grid. The elemental mapping and energy-dispersive X-ray spectroscopy (EDX) spectra were performed on a Hitachi Model S-4800 high-resolution fluorescence-emission

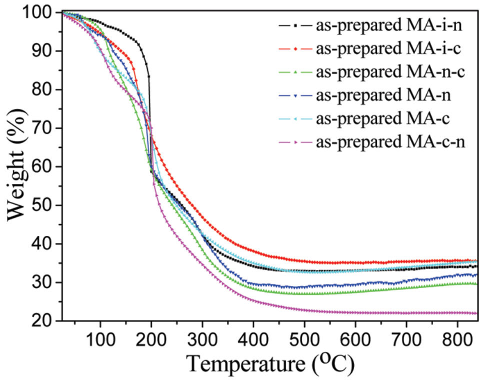

Figure 1. Thermogravimetric (TG) curves for alumina samples prepared from different aluminum salts.

scanning electron microscopy instrument, using an acceleration voltage of 30 kV.

2.3. Calculation. The specific surface areas (S_{BET}) were calculated from the N_2 adsorption isotherm in the relative pressure range of 0.05−0.2.[23] The single-point pore volume (V_{sp}) was estimated from the amount adsorbed at a relative pressure of ∼0.98. The pore size distributions (PSD) were calculated using adsorption branches of nitrogen adsorption−desorption isotherms by the improved KJS method calibrated for cylindrical pores.[24] The pore width (w_{KJS}) was obtained at the maximum of the PSD curve. The complementary pore volume (V_c) was evaluated by integration of the PSD curve up to ∼3 nm.

2.4. CO_2 and NH_3 TPD Measurements. To evaluate the acidic and basic sites of the selected MA and MA-supported metal oxides, CO_2 and NH_3 temperature-programmed desorption (TPD) experiments were conducted using a Micromeritics Auto Chem II Chemisorption Analyzer (Norcross, GA) that was equipped with a thermocouple detector (TCD). Approximately 0.15 g of each sample were loaded in a quartz tube microreactor supported by quartz wool and degassed at 500 °C for 2 h before CO_2 and 1 h before NH_3, using a heating rate of 5 °C/min in flowing helium (at a rate of 50 cm^3/min). Next, the samples were cooled to 120 °C and exposed to flowing 5% CO_2−He (50 cm^3/min) for 2.1 h and finally purged in flowing helium for 1 h; however, NH_3 chemisorption was done at 180 °C for 1.2 h. In the TPD experiments, the samples were heated up to 750 °C using a heating rate of 10 °C/min and kept at this temperature for 60 min in the case of CO_2 or up to 500 °C and kept at the latter temperature for 30 min in the case of NH_3. The amounts of desorbed CO_2 and NH_3 were obtained by integration of the desorption profiles and referenced to the TCD signals calibrated for known volumes of analyzed gases.

3. RESULTS AND DISCUSSION

3.1. Structural and Adsorption Properties of Ordered Mesoporous Aluminas. TG profiles recorded in air were first used to determine the thermal treatment temperature of the as-prepared composites prepared from different aluminum salts. Figure 1 and Figure S1 in the Supporting Information show that all the TG/DTG curves have three stages of the weight loss at different temperatures, and the highest weight losses are centered at ∼195 °C. The corresponding total weight losses for the MA-i-n, MA-i-c, MA-n-c, MA-n, MA-c, and MA-c-n samples are 65.9%, 64.4%, 70.4%, 68.0%, 64.6%, and 78.1%, respectively. In the case of the first step, ∼5.8−20.4% of the weight loss was observed up to 150 °C, which is attributable to the loss of physically adsorbed species such as water.[25] The second step represents the largest weight loss, ∼27.3−39.4%, located in the 150−225 °C range, which corresponds to the almost complete decomposition of the Pluronic P123 template. The third step represents the remaining weight loss of ∼19.5−25.2% located in the 225−750 °C range, which is attributed to the dehydroxylation of OH− groups and conversion of hydrated alumina into transitional alumina. The convincing evidence for the effective template removal from the as-prepared samples is provided by FT-IR spectra (Figure S2 in the Supporting Information). The absorption bands at ca. 1095, 1608, and 2970 cm^{-1} (Figure S2a in the Supporting Information) can be assigned to the C−O, C−C, and C−H bond stretching of the Pluronic P123 template, respectively. The absorption band at 1330 cm^{-1} provides also evidence for the presence of Pluronic P123. The absorption bands at 3126−3400, 1608, and 930 cm^{-1} may result from −OH stretching and bending vibrations of the hydrated alumina−Pluronic P123 composite surface.[26] The broadness of the absorption band at 3126−3400 cm^{-1} arises from intermolecular hydrogen bonding.[27] Note that after calcination at 400 °C in flowing air, the above bands almost completely disappeared (Figure S2b in the Supporting Information), giving evidence of the template removal and dehydration of hydrated alumina. A wide absorption band at ca. 3355 cm^{-1} corresponds to the bending vibration of hydrogen-bonded surface OH groups of the physically adsorbed water. The above FT-IR analysis is consistent with the TG results. The difference in the TG/DTG curves and FT-IR spectra among the samples may be due to the presence of water in $Al(NO_3)_3 \cdot 9H_2O$, and the effects of various combination of $Al(OC_3H_7)_3$, $Al(NO_3)_3 \cdot 9H_2O$, and $AlCl_3$ on the formation of the hydrated alumina−Pluronic P123 xerogels.

Effects of aluminum precursors on nitrogen adsorption isotherms and the corresponding pore size distributions of aluminum oxides are shown in Figure 2. The structural parameters derived from these isotherms are summarized in Table 1. All isotherms in Figure 2a are Type IV, which refers to mesoporous materials. The isotherms measured on the MA-i-c, MA-c-n, MA-i-n, and MA-c samples present H1 hysteresis loops, suggesting the presence of cylindrical mesopores. In the case of the MA-n and MA-n-c samples, desorption branches of nitrogen adsorption isotherms decline steeply at a relative pressure of ca. 0.45, giving large H2 hysteresis loops, which are characteristic for cagelike mesopores and/or mesopores with constrictions.[23] The well-developed H1 hysteresis loop in the case of MA-n and MA-n-c is believed to be related to the capillary condensation in large pore channels with possible channel modulation.[12] The steepness of the capillary condensation steps indicates a high degree of mesopore uniformity. The capillary condensation steps for the samples ranging from MA-i-c to MA-c-n, MA-i-n, MA-c, MA-n to MA-n-c are slightly shifted to greater relative pressures, indicating an increase in the size of mesopores. The corresponding pore size distribution (PSD) curves in Figure 2b are in accord with the adsorption isotherms in Figure 2a. For the adsorption isotherms with steep condensation steps (e.g., MA-c), the corresponding PSD curves represent narrow distributions. As can be seen from these figures, the textural properties of MA are highly dependent on the aluminum precursors used. The usage of $Al(NO_3)_3 \cdot 9H_2O$ as the main aluminum precursor led to the formation of MA (sample MA-n-c) with the largest mesopores (11.1 nm), while, in the case of $Al(OC_3H_7)_3$ as the main aluminum precursor (sample MA-i-c), small mesopores of ∼ 4.1 nm were observed (see Table 1). Also note that MA-i-n prepared from $Al(OC_3H_7)_3$−$Al(NO_3)_3 \cdot 9H_2O$ and MA-c prepared from $AlCl_3$ exhibited a high specific surface area of 530 m^2/g and a large pore

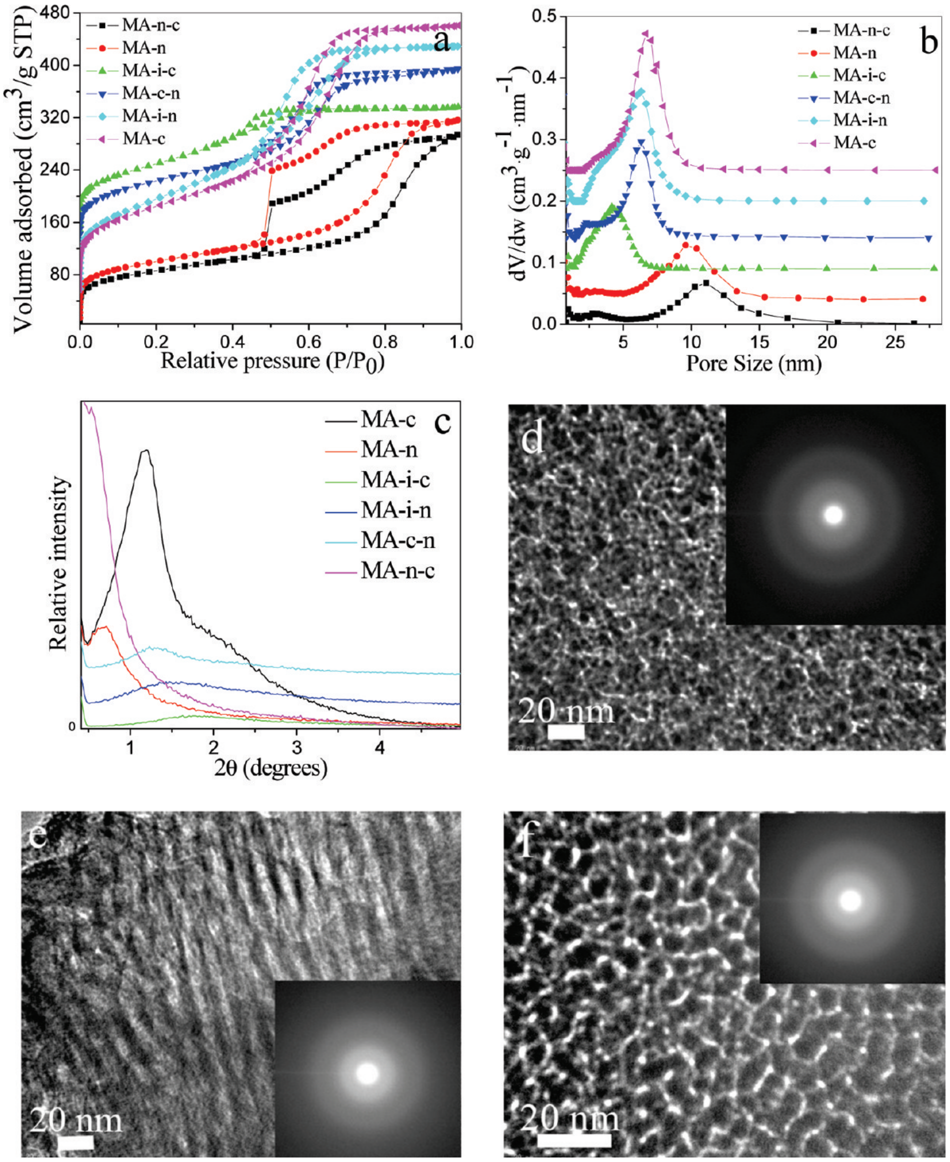

Figure 2. (a) Nitrogen adsorption isotherms, (b) the corresponding PSD curves, and (c) the small-angle XRD patterns for the MA samples prepared from different aluminum salts; TEM images and electron diffraction patterns of MA-i-n (d), MA-n (e), and MA-c (f). The isotherms for MA-n, MA-i-c, MA-c-n, MA-i-n, and MA-c (shown in panel a) are offset by 6, 140, 110, 50, and 50 cm^3 STP/g, respectively. The PSDs for MA-n, MA-i-c, MA-c-n, MA-i-n, and MA-c (shown in panel b) are offset by 0.04, 0.09, 0.14, 0.2, and 0.25 $cm^3/(g\ nm)$, respectively.

volume of 0.63 cm^3/g, respectively. However, as reported previously, the use of $Al(NO_3)_3 \cdot 9H_2O$ as an aluminum precursor and a citric acid additive resulted in aluminum oxide with a wider PSD and a lower specific surface area of 282 m^2/g, smaller pore volume of 0.38 cm^3/g, and smaller pore width of 3.6 nm.[15] Furthermore, Figures 2a and 2b show that a small amount of micropores exist in these mesoporous materials, possibly because of either a low extent of inclusion of PEO segments into the inorganic framework or the retraction of PEO chains under the present self-assembly conditions of the EISA process.[28]

The small-angle XRD patterns in Figure 2c indicate the presence of uniform mesoporosity. It is well-known that the diffraction patterns at small angles provide information about the possible organization of mesopores.[29] As can been seen in Figure 2c, the small-angle XRD patterns for the samples studied exhibit one peak at 2θ between 0.5° and 2.0°, indicating the presence of uniform mesopores, which can be ordered or wormlike. The increasing intensity of the small-angle peaks recorded for MA-n-c to MA-i-c, MA-i-n, MA-c-n, MA-n, and MA-c indicate the direction of the mesostructure improvement. The powder XRD patterns for MA-n calcined at 400, 700, and 900 °C (Figure S3 in the Supporting Information) also confirm good thermal stability of the resulting mesoporous alumina. The TEM image in Figure 2d shows that MA-i-n prepared from $Al(OC_3H_7)_3$—$Al(NO_3)_3 \cdot 9H_2O$ exhibits a spongelike mesoporous structure, which is somewhat similar to that of the MA prepared from $Al(s\text{-}BuO)_3$ in the presence of the anionic surfactant lauric acid and Pluronic L64.[30] However, the TEM images of MA-n prepared from $Al(NO_3)_3 \cdot 9H_2O$ (Figure 2e) and MA-c obtained from $AlCl_3$ (Figure 2f) show the presence of domains with ordered channel-like mesopores, which is in a good agreement with the intense XRD peak at small angles (Figure 2c). The TEM images also show that the channels are uniform, which corresponds to the pore width obtained from the adsorption data listed in Table 1. The electron diffraction

Table 1. Adsorption Parameters of MA and MA-Supported Metal Oxides Calcined at 400 °C for 4 h

sample	precursors		S_{BET} (m^2/g)[a]	V_{sp} (cm^3/g)[b]	V_c (cm^3/g)[c]	W_{KJS} (nm)[d]
MA-n-c	$Al(NO_3)_3 \cdot 9H_2O$	$AlCl_3$	307	0.45	0.032	11.1
MA-n	$Al(NO_3)_3 \cdot 9H_2O$		338	0.48	0.037	9.6
MA-i-c	$Al(OC_3H_7)_3$	$AlCl_3$	398	0.30	0.059	4.1
MA-c-n	$AlCl_3$	$Al(NO_3)_3 \cdot 9H_2O$	410	0.44	0.038	6.3
MA-i-n	$Al(OC_3H_7)_3$	$Al(NO_3)_3 \cdot 9H_2O$	530	0.59	0.033	6.3
MA-c	$AlCl_3$		489	0.63	0.014	6.6
MA-i-Ca	$Al(OC_3H_7)_3$	$Ca(NO_3)_2 \cdot 4H_2O$	328	0.26	0.068	5.7
MA-i-Fe	$Al(OC_3H_7)_3$	$Fe(NO_3)_3 \cdot 9H_2O$	409	0.28	0.082	4.2
MA-i-Mg	$Al(OC_3H_7)_3$	$Mg(NO_3)_2 \cdot 6H_2O$	214	0.41	0.004	11.6
MA-i-Cu	$Al(OC_3H_7)_3$	$Cu(NO_3)_2 \cdot 3H_2O$	432	0.43	0.062	6.3
MA-i-Ni	$Al(OC_3H_7)_3$	$Ni(NO_3)_2 \cdot 6H_2O$	548	0.60	0.033	6.0
MA-i-La*	$Al(OC_3H_7)_3$	$LaCl_3 \cdot 6H_2O$	363	0.30	0.036	4.6
MA-i-Y*	$Al(OC_3H_7)_3$	$YCl_3 \cdot 6H_2O$	372	0.35	0.022	5.4
MA-i-Ni*	$Al(OC_3H_7)_3$	$NiCl_2 \cdot 6H_2O$	340	0.38	0.011	5.6
MA-i-Sn*	$Al(OC_3H_7)_3$	$SnCl_4 \cdot 3H_2O$	523	0.38	0.086	4.2
MA-i-Cr*	$Al(OC_3H_7)_3$	$CrCl_3$	450	0.40	0.039	4.9
MA-i-Fe*	$Al(OC_3H_7)_3$	$FeCl_3$	393	0.42	0.031	6.0
MA-i-Ce*	$Al(OC_3H_7)_3$	$CeCl_3 \cdot 7H_2O$	456	0.49	0.016	5.2
MA-i-Cu*	$Al(OC_3H_7)_3$	$CuCl_2 \cdot 2H_2O$	339	0.51	0.000	7.0
MA-n-Sn*	$Al(NO_3)_3 \cdot 9H_2O$	$SnCl_4$	136	0.11	0.038	7.3
MA-n-Ca	$Al(NO_3)_3 \cdot 9H_2O$	$Ca(NO_3)_2 \cdot 4H_2O$	148	0.23	0.008	9.0
MA-n-Fe*	$Al(NO_3)_3 \cdot 9H_2O$	$FeCl_3$	252	0.29	0.069	15.9
MA-n-Ni	$Al(NO_3)_3 \cdot 9H_2O$	$Ni(NO_3)_2 \cdot 6H_2O$	282	0.37	0.030	8.9
MA-n-Cu	$Al(NO_3)_3 \cdot 9H_2O$	$Cu(NO_3)_2 \cdot 3H_2O$	335	0.41	0.051	9.6
MA-n-Cr*	$Al(NO_3)_3 \cdot 9H_2O$	$CrCl_3$	295	0.42	0.025	11.0
MA-n-Mg	$Al(NO_3)_3 \cdot 9H_2O$	$Mg(NO_3)_2 \cdot 6H_2O$	348	0.45	0.039	9.7
MA-c-Fe	$AlCl_3$	$Fe(NO_3)_3 \cdot 9H_2O$	241	0.16	0.060	2.0, 5.4
MA-c-Fe*	$AlCl_3$	$FeCl_3$	305	0.21	0.072	2.3, 5.5
MA-c-Cr*	$AlCl_3$	$CrCl_3$	419	0.48	0.022	2.7, 6.7
MA-c-Ni	$AlCl_3$	$Ni(NO_3)_2 \cdot 6H_2O$	384	0.50	0.023	2.3, 7.0
MA-c-Cu*	$AlCl_3$	$CuCl_2 \cdot 2H_2O$	395	0.55	0.041	2.9, 9.0
MA-c-Cu	$AlCl_3$	$Cu(NO_3)_2 \cdot 3H_2O$	420	0.70	0.013	3.8, 8.9

[a] Specific surface area calculated from adsorption data in the relative pressure range of 0.05−0.2. [b] Single-point pore volume calculated from the adsorption isotherm at the relative pressure of 0.98. [c] Complementary pore volume calculated by integration of the PSD curve up to ~3 nm. [d] Pore width calculated at the maximum of PSD, using the improved KJS method.

patterns (see insets in Figures 2d−f) confirm that the mesopore walls are polycrystalline, which is reflected by characteristic diffuse electron diffraction rings. However, the diffraction rings are rather weak and diffusive, revealing that the crystalline perfection of the samples is low. The partially ordered MA was prepared in the similar way by employing aluminum tri-*tert*-butoxide as the main inorganic precursor and anhydrous aluminum chloride as the pH adjustor and hydrolysis−condensation controller in tetrahydrofuran media.[13]

The EDX measurements were further conducted to determine the elemental constituents of the typical ordered MA. The homogeneous distribution of the elements within the framework of MA-i-n, MA-n, and MA-c was confirmed by the density of the O and Al spots in the elemental mapping (Figure S4 in the Supporting Information). Semiquantitative composition analyses indicate that the atomic ratio of O and Al is 2.0, 2.3, and 1.4, respectively, which is close to the theoretical value 1.5:1 of alumina (Table S1 in the Supporting Information), considering the effects of thermal treatment and the instrumental error. The possible phase segregation and different crystallization could locally alter the composition of these elements during the thermal treatment.[31] However, for MA-c prepared from $AlCl_3$, a small amount of Cl (6.8 at. %) was detected. The residual Cl may be related with the generation of the coordinated complex $AlCl_2(OC_3H_5) \cdot (AlCl_3)_2 \cdot 10C_2H_5OH$, accompanied by volatile HCl, during the alcoholysis process of $AlCl_3$.[32]

3.2. Adsorption and Structural Properties of Ordered Mesoporous Alumina-Supported Metal Oxides. To demonstrate the applicability of the approach to the synthesis of ordered MA-supported metal oxides, alumina samples containing nickel, magnesium, copper, chromium, iron, calcium, cerium, lanthanum, yttrium, and tin oxides were also prepared and characterized by nitrogen adsorption, small angle XRD and TEM (see Figures 3 and 4 in this work and Figures S5 and S6 in the

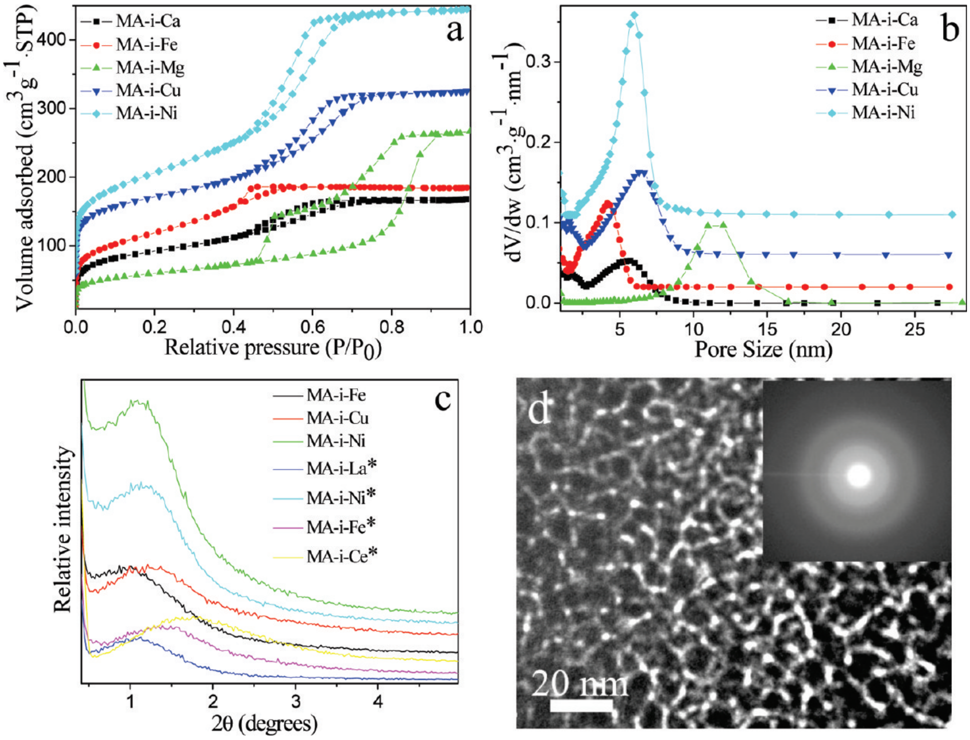

Figure 3. (a) Nitrogen adsorption isotherms, (b) the corresponding PSD curves for the MA-supported metal oxides prepared from Al(OC_3H_7)$_3$-Me nitrate, and (c) the small-angle XRD patterns for the oxides prepared from Al(OC_3H_7)$_3$-Me nitrate and Al(OC_3H_7)$_3$-Me chloride, respectively; (d) TEM image and electron diffraction pattern of MA-i-Ni. The isotherms for MA-i-Fe, MA-i-Mg, MA-i-Cu, and MA-i-Ni (panel a) are offset by 5.5, 0, 50, and 55 cm^3 STP/g, respectively. The PSD curves for MA-i-Fe, MA-i-Mg, MA-i-Cu, and MA-i-Ni (panel b) are offset by 0.02, 0, 0.06, and 0.11 cm^3/(g nm), respectively.

Supporting Information). Similar to the as-prepared ordered MA, all the isotherms measured on the supported-MA metal oxides are Type IV.[23] Except for the adsorption isotherms for MA-n-Sn* and MA-n-Fe*, which show relatively small adsorption, broad capillary condensation steps, and broad PSD curves (Figures 4a and 4b), all the remaining isotherms exhibit steep capillary condensation steps, which indicate the presence of uniform mesopores. Specifically, for the samples prepared from Al(OC_3H_7)$_3$-Me nitrate (Figures 3a and 3b), their isotherms exhibit H1 hysteresis loops, except for the isotherm for MA-i-Mg with a large H2 hysteresis loop. The condensation steps gradually shift to higher relative pressures, according to the following order: MA-i-Fe, MA-i-Ca, MA-i-Ni, MA-i-Cu, and MA-i-Mg, indicating the direction of increase, relative to the size of mesopores. Especially, MA-i-Mg shows the largest pore width of 11.6 nm (Table 1). Therefore, in comparison to other nitrates, the addition of $Mg(NO_3)_2 \cdot 6H_2O$ into the ethanol solution of Al(OC_3H_7)$_3$ seems to be an effective way for increasing the pore size of the resulting Mg-MA sample. However, the isotherm for MA-i-Ni shows the highest and steepest condensation, indicating large pore volume (0.60 cm^3/g) and highly uniform mesopores.

In the case of the samples prepared from Al(OC_3H_7)$_3$-Me chloride (see Figures S5a and S5b in the Supporting Information), there is no pronounced difference in the steepness and position of capillary condensation steps, except for MA-i-Cu*. The latter sample shows the steepest capillary condensation step, which is the closest to the relative pressure (P/P_0) of 1. Small-angle XRD patterns for selected samples prepared from Al(OC_3H_7)$_3$-Me nitrate and Al(OC_3H_7)$_3$-Me chloride exhibit only one small-angle wide peak (Figure 3c), indicating their wormlike or sponge-like mesostructure. The typical TEM image (Figure 3d) of MA-i-Ni prepared from Al(OC_3H_7)$_3$–$Ni(NO_3)_2 \cdot 6H_2O$ shows that the incorporation of nickel into aluminum oxide does not change the wormlike polycrystalline structure with uniform channels.

For the samples prepared from aluminum nitrate-Me nitrate and aluminum nitrate-Me chloride, except for MA-n-Sn*, MA-n-Fe*, and MA-n-Cu having adsorption isotherms with H1 hysteresis loops, the incorporation of Ca, Ni, Cr, and Mg into the aluminum oxide does not change the isotherms shape with a large H2 hysteresis loop (see Figures 4a and 2a). However, in comparison to other aluminum precursors, the use of aluminum nitrate as the main aluminum precursor results in MA-supported metal oxides with larger pores centered at ∼7.3–15.9 nm, which is reflected by appearance of the capillary condensation steps at higher relative pressures. Furthermore, the specific surface area and pore volume vary much from MA-n-Sn* (136 m^2/g and 0.11 cm^3/g) to MA-n-Mg (348 m^2/g and 0.45 cm^3/g). Figure 4c shows the tendency of increasing intensity of the small-angle XRD peak in the sequence from MA-n-Cu to MA-n-Cr*, MA-n-Mg, and MA-n-Ni, indicating the direction of increasing ordering in these mesostructures. For selected MA-n-Ni and MA-n-Mg samples, Figures 4d and 4e, in combination with Figure 4c, clearly show the efficient formation of ordered mesostructures with polycrystalline pore walls.

Unlike the MA-supported metal oxides prepared from aluminum nitrate-Me chloride and aluminum nitrate-Me nitrate, all isotherms of the MA-supported metal oxides prepared from aluminum chloride-Me chloride and aluminum nitrate-Me nitrate (see Figure S6a in the Supporting Information) are Type IV

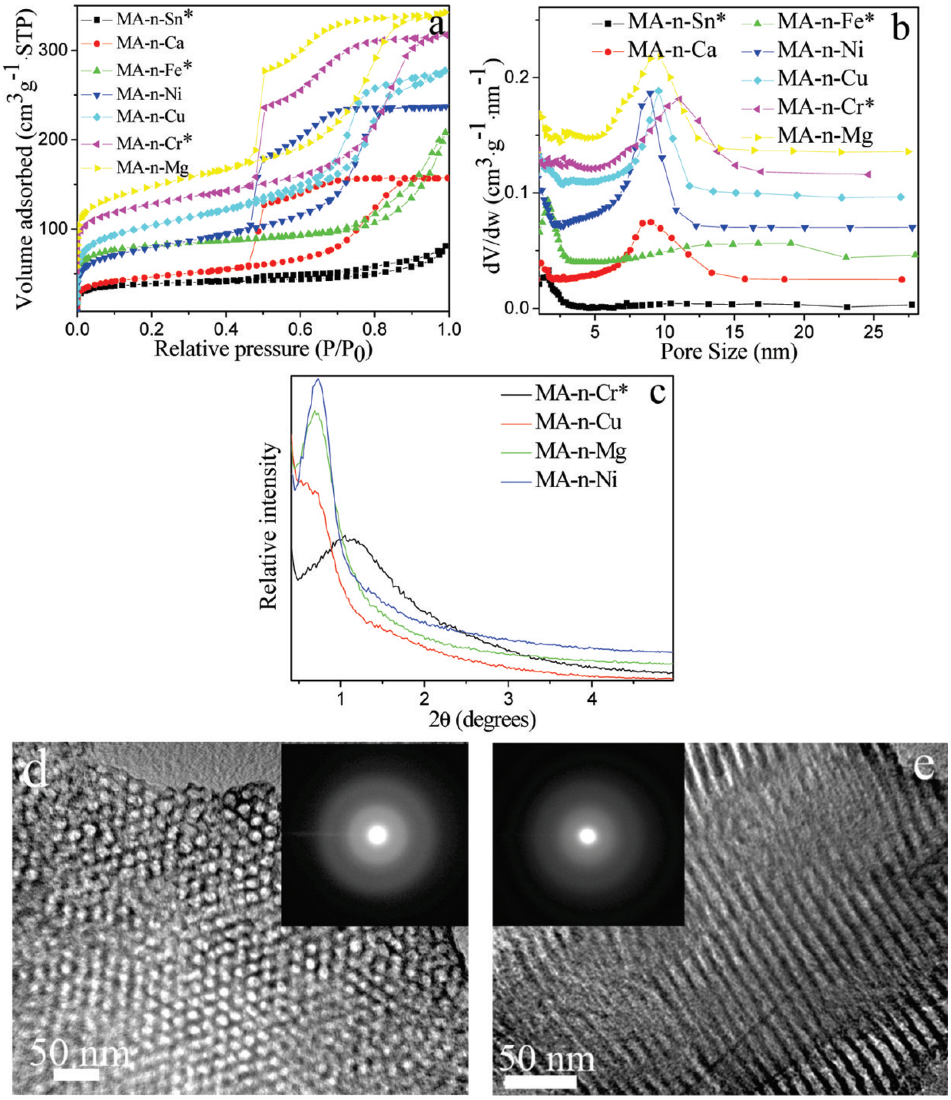

Figure 4. (a) Nitrogen adsorption isotherms, (b) the corresponding PSD curves, and (c) the small-angle XRD patterns for the MA-supported metal oxides prepared from aluminum nitrate-Me nitrate and aluminum nitrate-Me chloride respectively; TEM images and electron diffraction patterns of MA-n-Ni (d) and MA-n-Mg (e). The isotherms for MA-n-Ca, MA-n-Fe*, MA-n-Ni, MA-n-Cu, MA-n-Cr*, and MA-n-Mg (panel a) are offset by 5, 10, 0, 10, 45, and 50 cm^3 STP/g, respectively. The PSD curves for MA-n-Ca, MA-n-Fe*, MA-n-Ni, MA-n-Cu, MA-n-Cr*, and MA-n-Mg (panel b) are offset by 0.025, 0.04, 0.07, 0.095, 0.115, and 0.135 cm^3/(g nm), respectively.

with two relatively well-separated condensation steps, which indicate the presence of two distinct types of pores in these samples.[33] Accordingly, the peaks of the bimodal PSD curves vary over ranges of 2.0−3.8 and 5.4−9.0 nm, respectively (see Figure S6b in the Supporting Information). The small mesopores inside the frameworks may be caused by the distortion of surfactant micelles upon heating.[28] However, for the MA-supported metal oxides prepared from aluminum nitrate-Me chloride and aluminum nitrate-Me nitrate, small mesopores are pronounced, in addition to large mesopores developed after the introduction of $Fe(NO_3)_3 \cdot 9H_2O$, $FeCl_3$, $CrCl_3$, $Ni(NO_3)_2 \cdot 6H_2O$, $CuCl_2 \cdot 2H_2O$, and $Cu(NO_3)_2 \cdot 3H_2O$. For instance, MA-c-Cu has a large pore volume of 0.70 cm^3/g and a high specific surface area of 420 m^2/g.

The expected presence of O, Al, and incorporated metal elements was confirmed by EDX analysis. For example, three regions of MA-i-Ni were scanned, and O, Al, and traces of Ni were found. These elements are distributed homogeneously throughout the sample (see Figure 5). The atomic ratios of O, Al, and Ni, analyzed in the three regions, are 2.18:1.00:0.13, 1.77:1.00:0.08, and 2.15:1.00:0.12, respectively. In comparison with the theoretical 1.00/0.10 molar ratio of Al/Ni in the precursor solutions, this ratio in the final oxide varies slightly, depending on the sampled region. The density of the O, Al and Me elements in the elemental mappings of MA-n-Ni, MA-n-Mg, and MA-c-Ni also confirm that these elements are distributed uniformly within the inorganic framework (see Figures S7 and S8 in the Supporting Information). Moreover, similar to MA-c prepared from $AlCl_3$, a small amount of chlorine (4.4 at.%) was detected in MA-c-Ni (see Table S1 in the Supporting Information). In contrast, the use of aluminum isopropoxide and aluminum nitrate as aluminum precursors does not introduce any impurity into the MA-supported metal oxides. Thus, the atomic-level homogeneity of the MA-supported metal oxides framework was clearly achieved by controlling the amount of the aforementioned Me nitrates and Me

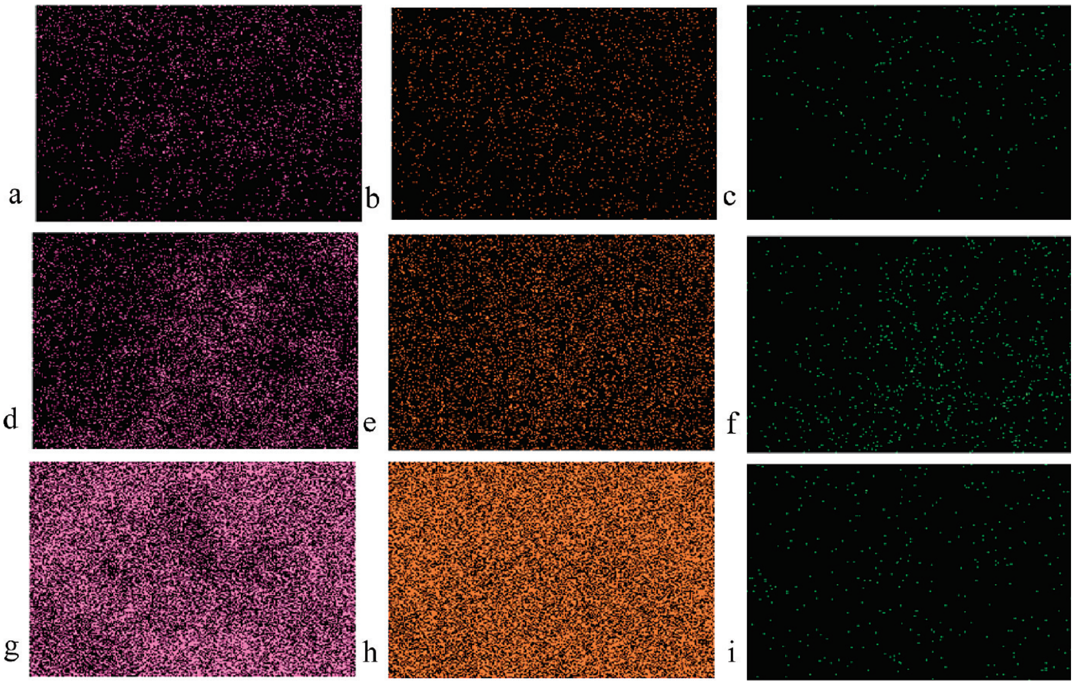

Figure 5. Elemental analysis maps for MA-i-Ni analyzed in three regions containing different percentages of (a, d, g) O, (b, e, h) Al, and (c, f, i) Ni. Maps in each row were made for the same region. For the first row, the atomic ratio of O/Al/Ni is 2.18:1.00:0.13; for the second row, the ratio is 1.77:1.00:0.08; and for the third row, the ratio is 2.15:1.00:0.12.

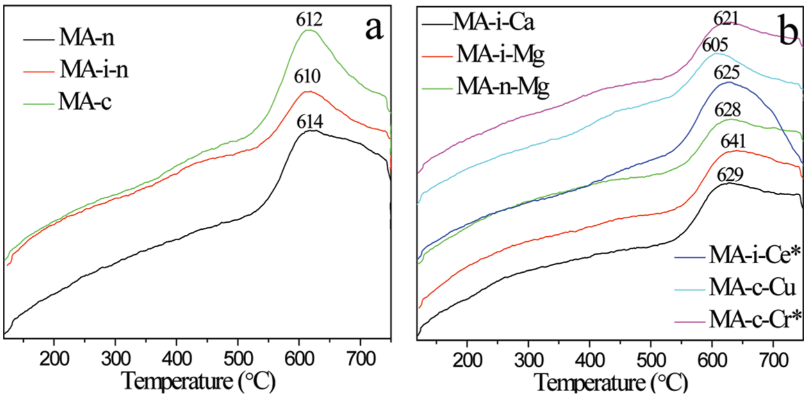

Figure 6. CO_2-TPD profiles for (a) selected MAs and (b) their supported-metal oxide samples.

chlorides added to aluminum precursors without any addition of water and acids.

3.3. CO_2 and NH_3 Adsorption Behavior. The CO_2-TPD and NH_3-TPD profiles were recorded to show the difference in the strength and the amount of basic and acidic sites of the selected MA and MA-supported metal oxides, and γ-Al_2O_3 obtained from the commercial boehmite powder; these profiles are shown in Figures 6 and 7, respectively (CO_2- and NH_3-TPD profiles also are shown in Figures S9−S12 in the Supporting Information; the basicity and acidity data are summarized in Tables S2 and S3 in the Supporting Information). The CO_2-TPD profiles in Figure 6 show a broad peak, indicating the existence of a wide range of basic sites on the surface of the samples studied. Considering that the weights of the MA samples were almost constant after 500 °C (see Figure 1), the possible dehydration at higher temperatures was considered as negligible. Furthermore, the main desorption peaks of the commercial γ-Al_2O_3 and γ-Al_2O_3 obtained from commercial boehmite after calcination at 400 °C are located at 620 °C[25b] and 642 °C (see Figure S12a in the Supporting Information), respectively. Therefore, the high-temperature desorption in the range of 605−641 °C can be related to CO_2 chemisorption. It should be noted that the desorption peak for the samples MA-i-Ca, MA-i-Mg and MA-n-Mg centers at 629, 641, and 628 °C, respectively, indicating little stronger basic sites than those on the samples without Ca or Mg, whose desorption peak centers at 605−625 °C. The use of $Al(NO_3)_3 \cdot 9H_2O$ as the sole aluminum precursor gave MA with the maximum CO_2 desorption amount of 1361.2 μmol/g. However, the sample MA-i-Mg prepared from $Al(OC_3H_7)_3$−$Mg(NO_3)_2 \cdot 6H_2O$ has a maximum percentage of active surface area of 62.6% (see Table S2 in the Supporting Information). It is interesting that there is some similarity between the CO_2-TPD measurements for the selected MA and MA-supported metal oxide samples (desorption peaks centered

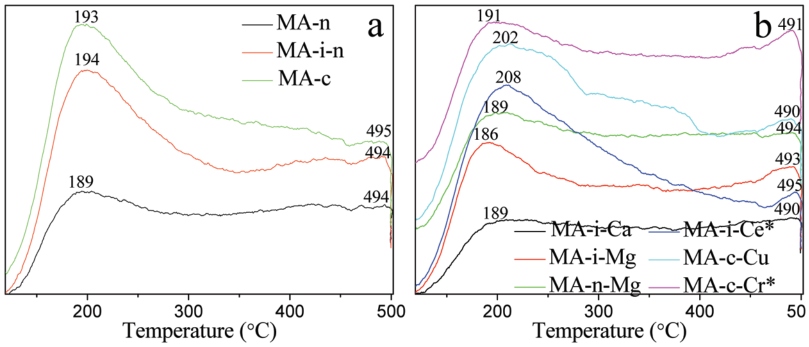

Figure 7. NH_3-TPD profiles for (a) selected MAs and (b) their supported-metal oxide samples.

at ~458 and 744 °C; see Figure S11 in the Supporting Information), and for γ-Al_2O_3 obtained from commercial boehmite after calcination at 700 °C (desorption peaks centered at ~454 and 740 °C; see Figure S12a). In contrast, the numbers of basic sites become higher than those for the MA and MA-supported metal oxide samples after calcination at 400 °C, except for the γ-Al_2O_3 sample obtained from commercial boehmite (see Table S2 in the Supporting Information). This difference may be due to subtle nanostructural changes that occur at the first surface/subsurface layers of the mesoporous oxides.[25c] Apparently, the numbers of basic sites for the selected samples are greatly higher, in comparison to the alkoxide-, commercial boehmite-based MA with Pluronic P123 as the template and nitric acid as pH adjustor, and three-dimensionally ordered macroporous MgO and γ-Al_2O_3 templated by triblock copolymer $EO_{106}PO_{70}EO_{106}$ (Pluronic F127) and regularly packed monodispersive polymethyl methacrylate microspheres.[25]

The NH_3-TPD profiles in Figure 7 show two distinct desorption peaks, which center at 186−208 °C and 490−495 °C, respectively. The former peak is attributed to weakly adsorbed NH_3 species, while the latter peak is assigned to strongly adsorbed NH_3 species. The selected MA samples, obtained by using $AlCl_3$ as the sole aluminum precursor, gave MA with a maximum NH_3 desorption amount of 540.6 μmol/g and percentage of active surface area of 9.3%, while the selected MA-supported metal oxides (for instance, the sample MA-i-Ce* prepared from $Al(OC_3H_7)_3$−$CeCl_3 \cdot 7H_2O$) showed a maximum NH_3 desorption amount of 571.8 μmol/g and a percentage of active surface area of 10.6%. In contrast, the MA-n, MA-i-Ca, MA-i-Mg, and MA-n-Mg samples have less acidic sites, as a result of their better basic properties. Therefore, the number of basic and acidic sites is variable, indicating that the MA and MA-supported metal oxides studied are suitable for use as supports or adsorbents, and especially some of them may have application as CO_2 adsorbents.

3.4. Discussion. A guide for the selection of precursors in preparing alumina-based mesoporous metal oxides with various metal additives under nonaqueous conditions is the "acid−base" concept, which self-adjust the acidity and homogeneity of inorganic precursors.[13,34] The "acid−base" synthesis route has been used to prepare ordered mesoporous metal phosphates, metal borates, titania, and zirconia, and also alumina using inorganic metal or nonmetal chlorides as acids, and alkoxides and esters as bases. However, to the best of our knowledge, there is no any report in which nitrate is used as acid to synthesize mesoporous metal oxides in ethanol. Herein, a series of ordered MA and MA-supported metal oxides was prepared in ethanol using hydrated nitrates besides chlorides as the pH adjustor and hydrolysis−condensation controller without any acid additive. For aluminum chloride and other metal (Ni, Fe, Cr, Cu, Ce, La, Y, and Sn) chlorides, they can react with ethanol, producing in situ chloroalkoxide and HCl, and thus slowing the condensation process of crown-ether-type complexes formed by alkylene oxide segments of Pluronic P123 with metal species through coordination bonds.[12,17] For aluminum nitrate nonahydrate and other metal (Ni, Mg, Fe, Cu, and Ca) nitrates containing crystallographic water, although they cannot react with ethanol, they are also acidic precursors. These nitrates can hydrolyze and produce H^+ in situ, because of the transformation of the crystallographic water to free water in nitrate. The trace water in ethanol and the relative humidity in the air above the solution may also have an effect on the hydrolysis process of nitrates.

It was reported that the reaction rate and the assembly process of the silicate−surfactant mesophase are greatly influenced by the radius and charge of anions such as Cl^-, I^-, and NO_3^-.[35] In the case of this system, NO_3^- has a larger aqueous ionic radius (206 pm) than that of the Cl^- (183 pm), and its complexation ability is weaker than that of the Cl^-.[15,36] Cl^- ions can strongly coordinate with Al ions and might destroy the balance at the organic/inorganic interface and disturb the assembly process. However, the NO_3^- ion does not strongly influence the self-assembly process, leading to ordered mesostructures.[37] Because the alcoholysis of chloride in ethanol is violent and the volatility of HCl is higher than that of HNO_3, the acidity of the entire system, in the case of aluminum chloride and other metal chlorides as precursors in an evaporation process, is reduced more quickly. However, when aluminum nitrate nonahydrate and other hydrated metal nitrates were used as precursors, the hydrolysis of nitrate is comparatively limited, because of the slow transformation of the crystallographic water to free water and the extremely limited amount of water from air above the solution.[28] Therefore, they act as sustained-release agents to maintain an acidic equilibrium environment, and, thus, consequently result in final products with larger mesoporous sizes and better ordering. Tang et al. found an order of SO_4^{2-} (HSO_4^-) > NO_3^- > Cl^- in acidic solutions to cause the transformation from *p6m* to *Ia*3*d* mesostructure when triblock copolymer Pluronic P123 is employed as a template. This order is different from either the Hofmeister series or the reverse, which can be attributed to the balance between dehydration and radii effects.[38] Furthermore, the mesostructures obtained from chloride salts are more disordered than those prepared from $Al(NO_3)_3$, which may be related to the fact that some incorporation of chloride ions into the mesostructure was observed in contrast to nitrate ions (see Table S1). This incorporation may affect the pore-forming mechanism and lead to different textural properties of the resulting MA.[37] As for $Al(OC_3H_7)_3$, it is assigned as base and extra oxygen donor, because no acid substances are generated when it reacts very slowly with ethanol. Therefore, a certain amount of $Al(OC_3H_7)_3$ is not only beneficial for tuning the acidity, but also crucial for achieving a homogeneous composition within the entire framework. As a polar solvent, ethanol can improve the proton transfer within the system, because of its oxygen-donating property, and thus promotes the inorganic—inorganic polymerization needed for assembly of mesostructured oxide materials. The PEO-PPO-PEO block copolymer (P123) could not only stabilize the Al and other metal species through complexation bonds, but also inhibits agglomeration of alumina nanoparticles.[39] Consequently, the polymerization, condensation, cross-linking and gelation of homogeneous aluminum and other incorporated metal precursors around the Pluronic P123 micelles during ethanol evaporation may occur easier. Also, the differences in the structure, textural, basic, and acidic properties of the final materials can be associated with interfacial interactions between different components in the mesostructures studied. Namely, the ionic strength, counterion polarizability, counterion charge, complexation ability of aluminum ions, metal precursors, Pluronic P123 concentration, and other factors may suppress the crystallization and growth of individual components by limiting diffusion in the certain synthesis mixtures.[15,40]

On the basis of these results, it is concluded that, in the systems studied, aluminum and the incorporated metal precursors are key factors in obtaining mesostructured phases with tailored adsorption and framework properties, while the introduction of the aforementioned metal species does not affect the formation of mesoporous structures. For example, large-pore mesoporous oxides with an ordered mesostructure and bimodal mesoporous oxides with high specific surface area are easily prepared using $Al(NO_3)_3 \cdot 9H_2O$ and $AlCl_3$ as the main aluminum precursors, respectively. Furthermore, although the most of these mesoporous materials show only one broad small angle XRD peak and they are less ordered compared to their silica counterparts, they have uniformly sized mesopores, high surface areas, and distinct basic-acidic properties, the key characteristics for adsorption and catalysis-related applications.

4. CONCLUSIONS

In summary, the use of aluminum isopropoxide, aluminum chloride, and aluminum nitrate nonahydrate as aluminum sources, and various metal (Ni, Mg, Fe, Cr, Cu, Ce, La, Y, Ca and Sn) chlorides or nitrates as modifiers afforded ordered mesoporous alumina (MA) and MA-supported metal oxides via Pluronic P123-assisted ethanol evaporation-induced self-assembly strategy without the addition of any acid. The resulting oxides show well-defined mesostructures, high surface areas, uniform pore sizes, tunable ordering, homogeneous framework compositions, and enhanced basic and acidic properties. Especially, mesoporous metal oxides prepared from aluminum nitrate exhibit good ordered mesostructures, larger mesopores (centering at 6.3—15.9 nm), and better adsorption performance of CO_2 than the oxides prepared from aluminum chloride and aluminum isopropoxide, and the MA materials reported previously. If an incomplete elimination of chloride upon calcination in the samples prepared from chlorides, and the cost and toxicity of aluminum alkoxides, are further considered, aluminum nitrate nonahydrate is the most suitable aluminum precursor for the synthesis of MA and MA-supported metal oxides. This finding permits the synthesis of ordered MA and MA-supported metal oxides without aluminum alkoxide, which results in a significant cost reduction when aluminum chloride and especially aluminum nitrate nonahydrate are used as the aluminum source.

■ ASSOCIATED CONTENT

Ⓢ **Supporting Information.** Twelve figures showing FT-IR spectra, small angle XRD patterns, wide-angle XRD patterns, elemental analysis maps, nitrogen adsorption isotherms, PSD curves, CO_2 adsorption profiles, and NH_3 adsorption profiles for the selected MA and MA-supported metal oxides, and for γ-Al_2O_3 obtained from commercial boehmite powder; and three tables showing the elemental constituents and the basicity and acidity data of the selected MA and MA-supported metal oxides. This material is available free of charge via the Internet at http://pubs.acs.org.

■ AUTHOR INFORMATION

Corresponding Author

*Tel.: +86-27-8787 1029 (J.Y.). Fax: +86-27-8787 9468 (J.Y.).
E-mail: jiaguoyu@yahoo.com (J.Y.).
*Tel.: +1-330-672 3790 (M.J.). Fax. +1-330-672 3816 (M.J.).
E-mail: jaroniec@kent.edu (M.J.).

■ ACKNOWLEDGMENT

The China Scholarship Council is acknowledged for support of this research under the State Scholarship Fund Program.

■ REFERENCES

(1) Trueba, M.; Trasatti, S. P. *Eur. J. Inorg. Chem.* **2005**, No. 17, 3393.

(2) Trimm, D. L.; Stanislaus, A. *Appl. Catal.* **1986**, *21*, 215.

(3) (a) Yuan, Z.-Y.; Ren, T.-Z.; Vantomme, A.; Su, B.-L. *Chem. Mater.* **2004**, *16*, 5096. (b) Danks, T. N.; Desai, B. *Green Chem.* **2002**, *4*, 179.

(4) (a) Cai, W. Q.; Yu, J. G.; Mann, S. *Microporous Mesoporous Mater.* **2009**, *122*, 42. (b) Cai, W. Q.; Yu, J. G.; Cheng, B.; Jaroniec, M. *J. Phys. Chem. C* **2009**, *113*, 14739. (c) Cai, W. Q.; Yu, J. G.; Gu, S. H.; Jaroniec, M. *Cryst. Growth Des.* **2010**, *10*, 3977.

(5) Yu, X. X.; Yu, J. G.; Cheng, B.; Jaroniec, M. *J. Phys. Chem. C* **2009**, *113*, 17527.

(6) (a) Čejka, J. *Appl. Catal., A* **2003**, *254*, 327. (b) Márquez-Alvarez, C.; Žilková, N.; Pérez-Pariente, J.; Čejka, J. *Catal. Rev.* **2008**, *50*, 222.

(7) (a) Bejenaru, N.; Lancelot, C.; Blanchard, P.; Lamonier, C.; Rouleau, L.; Payen, E.; Dumeignil, F; Royer, S. *Chem. Mater.* **2009**, *21*, 522. (b) Zhang, Z. R.; Pinnavaia, T. J. *Langmuir* **2010**, *26*, 10063. (c) Dong, A. G.; Ren, N.; Tang, Y.; Wang, Y. J.; Zhang, Y. H.; Hua, W. M.; Gao, Z. *J. Am. Chem. Soc.* **2003**, *125*, 4976.

(8) Voort, P. V. D.; Vercaemst, C.; Schaubroeck, D.; Verpoort, F. *Phys. Chem. Chem. Phys.* **2008**, *10*, 347.

(9) Lee, J.; Orilall, M. C.; Warren, S. C.; Kamperman, M.; DiSalvo, F. J.; Wiesner, U. *Nat. Mater.* **2008**, *7*, 222.

(10) Kim, Y.; Kim, C.; Choi, I.; Rengaraj, S.; Yi, J. *Environ. Sci. Technol.* **2004**, *38*, 924.

(11) Vaudry, F.; Khodabandeh, S.; Davis, M. E. *Chem. Mater.* **1996**, *8*, 1451.

(12) Yang, P. D.; Zhao, D. Y.; Margolese, D. I.; Chmelka, B. F.; Stucky, G. D. *Nature* **1998**, *396*, 152.

(13) (a) Tian, B. Z; Yang, H. F.; Liu, X. Y.; Xie, S. H.; Yu, C. Z.; Fan, J.; Tu, B.; Zhao, D. Y. *Chem. Commun.* **2002**, No. 17, 1824. (b) Tian,

B. Z.; Liu, X. Y.; Tu, B.; Yu, C. Z.; Fan, J.; Wang, L. M.; Xie, S. H.; Stucky, G. D.; Zhao, D. Y. *Nat. Mater.* **2003**, *2*, 159.

(14) Niesz, K.; Yang, P. D.; Somorjai, G. A. *Chem. Commun.* **2005**, No. 15, 1986.

(15) Yuan, Q.; Yin, A. X.; Luo, C.; Sun, L. D.; Zhang, Y. W.; Duan, W. T.; Liu, H. C.; Yan, C. H. *J. Am. Chem. Soc.* **2008**, *130*, 3465.

(16) Dacquin, J. P.; Dhainaut, J.; Duprez, D.; Royer, S.; Lee, A. F.; Wilson, K. *J. Am. Chem. Soc.* **2009**, *131*, 12896.

(17) Wan, Y.; Shi, Y. F.; Zhao, D. Y. *Chem. Commun.* **2007**, No. 9, 897.

(18) Wang, G. Z.; Zhang, L.; Dai, H. X.; Deng, J. G.; Liu, C. X.; He, H.; Au, C. T. *Inorg. Chem.* **2008**, *47*, 4015.

(19) Kaluža, L.; Gulkova′, D.; Šolcová, O.; Žilková, N.; Čejka, J. *Appl. Catal., A* **2008**, *351*, 93.

(20) Sun, L. B.; Tian, W. H.; Liu, X. Q. *J. Phys. Chem. C* **2009**, *113*, 19172.

(21) Kim, P.; Kim, Y.; Kim, H.; Song, I. K.; Yi, J. *Appl. Catal., A* **2004**, *272*, 157.

(22) Morris, S. M.; Fulvio, P. F.; Jaroniec, M. *J. Am. Chem. Soc.* **2008**, *130*, 15210.

(23) Kruk, M.; Jaroniec, M. *Chem. Mater.* **2001**, *13*, 3169.

(24) Jaroniec, M.; Solovyov, L. *Langmuir* **2006**, *22*, 6757.

(25) (a) Fulvio, P. F.; Pikus, S.; Jaroniec, M. *ACS Appl. Mater. Interfaces* **2010**, *2*, 134. (b) Li, H. N.; Zhang, L.; Dai, H. X.; He, H. *Inorg. Chem.* **2009**, *48*, 4421. (c) Boukha, Z.; Fitian, L.; López-Haro, M.; Mora, M.; Ruiz, J. R.; Jiménez-Sanchidrián, C.; Blanco, G.; Calvino, J. J.; Cifredo, G. A.; Trasobares, S.; Bernal, S. *J. Catal.* **2010**, *272*, 121.

(26) (a) Lu, C. L.; Lv, J. G.; Xu, L.; Guo, X. F.; Hou, W. H.; Hu, Y.; Huang, H. *Nanotechnology* **2009**, *20*, 215604. (b) Bai, P.; Su, F.; Wu, P.; Wang, L.; Lee, F. Y.; Lv, L.; Yan, Z.-F.; Zhao, X. S. *Langmuir* **2007**, *23*, 4599.

(27) Meng, Y.; Gu, D.; Zhang, F. Q.; Shi, Y. F.; Cheng, L.; Feng, D.; Wu, Z. X.; Chen, Z. X.; Wan, Y.; Stein, A.; Zhao, D. Y. *Chem. Mater.* **2006**, *18*, 4447.

(28) Wan, Y.; Zhao, D. Y. *Chem. Rev.* **2007**, *107*, 2821.

(29) Rashidi, F.; Kharat, A. N.; Rashidi, A. M.; Lima, E.; Lara, V.; Valente, J. S. *Eur. J. Inorg. Chem.* **2010**, *10*, 1544.

(30) Caragheorgheopol, A.; Rogozea, A.; Ganea, R.; Florent, M.; Goldfarb, D. *J. Phys. Chem. C* **2010**, *114*, 28.

(31) Fulvio, P. F.; Vinu, A.; Jaroniec, M. *J. Phys. Chem. C* **2009**, *113*, 13565.

(32) Zhang, J.; Liu, S.; Lin, J.; Song, H.; Luo, J.; Elssfah, E. M.; Ammar, E.; Huang, Y.; Ding, X.; Gao, J.; Qi, S.; Tang, C. *J. Phys. Chem. B* **2006**, *110*, 14249.

(33) Kruk, M.; Matos, J. R.; Jaroniec, M. *Colloids Surf. A* **2004**, *241*, 27.

(34) Wan, Y.; Yang, H. F.; Zhao, D. Y. *Acc. Chem. Res.* **2006**, *39*, 423.

(35) Zhao, D. Y.; Huo, Q. S.; Feng, J. L.; Chmelka, B. F.; Stucky, G. D. *J. Am. Chem. Soc.* **1998**, *120*, 6024.

(36) Cai, W. Q.; Yu, J. G.; Jaroniec, M. *J. Mater. Chem.* **2010**, *20*, 4587.

(37) Zhang, Z. R.; Pinnavaia, T. J. *J. Am. Chem. Soc.* **2002**, *124*, 12294.

(38) Tang, J. W.; Yu, C. Z.; Zhou, X. F.; Yan, X. X.; Zhao, D. Y. *Chem. Commun* **2004**, *19*, 2240.

(39) Liu, R. X.; Wu, C. Y.; Wang, Q.; Ming, J.; Hao, Y. F.; Yu, Y. C.; Zhao, F. Y. *Green Chem.* **2009**, *11*, 979.

(40) Li, D. L.; Zhou, H. S.; Honma, I. *Nat. Mater.* **2004**, *3*, 65.